A programmed surface on polyetheretherketone for sequentially dictating osteoimmunomodulation and bone regeneration to achieve ameliorative osseointegration under osteoporotic conditions

Yanyan Zheng [a,b,1], Ang Gao [a,1], Jiaxiang Bai [c,1], Qing Liao [a], Yuzheng Wu [d], Wei Zhang [e], Min Guan [a], Liping Tong [a,*], Dechun Geng [c,**], Xin Zhao [f], Paul K. Chu [d], Huaiyu Wang [a,***]

[a] Center for Human Tissues and Organs Degeneration, Shenzhen Institute of Advanced Technology, Chinese Academy of Sciences, Shenzhen, 518055, China
[b] School of Basic Medical Sciences and Forensic Medicine, North Sichuan Medical College, Nanchong, 637000, China
[c] Department of Orthopaedics, The First Affiliated Hospital of Soochow University, Suzhou, 215006, China
[d] Department of Physics, Department of Materials Science and Engineering, Department of Biomedical Engineering, City University of Hong Kong, Tat Chee Avenue, Kowloon, Hong Kong, China
[e] Technical Institute of Physics and Chemistry, Chinese Academy of Sciences, Beijing, 100190, China
[f] Department of Biomedical Engineering, The Hong Kong Polytechnic University, Hong Kong, China

ARTICLE INFO

ABSTRACT

Polyetheretherketone (PEEK) is a desirable alternative to conventional biomedical metals for orthopedic implants due to the excellent mechanical properties. However, the inherent bioinertness of PEEK contributes to inferior osseointegration of PEEK implants, especially under pathological conditions of osteoporosis. Herein, a programmed surface is designed and fabricated on PEEK to dictate osteoimmunomodulation and bone regeneration sequentially. A degradable hybrid coating consisting of poly(lactide-co-glycolide) and alendronate (ALN) loaded nano-hydroxyapatite is deposited on PEEK and then interleukin-4 (IL-4) is grafted onto the outer surface of the hybrid coating with the aid of N_2 plasma immersion ion implantation and subsequent immersion in IL-4 solution. Dominant release of IL-4 together with ALN and Ca^{2+} during the first few days synergistically mitigates the early acute inflammatory reactions and creates an osteoimmunomodulatory microenvironment that facilitates bone regeneration. Afterwards, slow and sustained delivery of ALN and Ca^{2+} in the following weeks boosts osteogenesis and suppresses osteoclastogenesis simultaneously, consequently ameliorating bone-implant osseointegration even under osteoporotic conditions. By taking into account the different phases in bone repair, this strategy of constructing advanced bone implants with sequential functions provides customizable and clinically viable therapy to osteoporotic patients.

1. Introduction

With the accelerated aging of population, more and more people are suffering from the degenerative orthopedic diseases, thus boosting the clinical demand of orthopedic implants. As an alternative to biomedical metals, polyetheretherketone (PEEK) is promising in orthopedics on account of outstanding attributes such as the excellent mechanical properties, intrinsic radiolucency, and sufficient biostability [1,2]. More importantly, the elastic modulus of PEEK is analogous to that of human cortical bone thus circumventing the stress shielding effects that plague metallic implants and consequently avoiding peri-implant osteanabrosis. However, despite these advantages, the bioinertness of pristine PEEK hinders integration with native bone tissues *in vivo* and so improvement is needed [3]. To enhance the osseointegration ability of PEEK prostheses, surface modification strategies such as electron beam evaporation [4], plasma treatment [5–7], and wet chemistry [8–10]

---

have been proposed. Although some progress has been made, most of the current studies only focus on the regulation of osteoblastic lineage cells but ignore the effects of other critical factors such as the host immune response which can determine the fate of implanted biomaterials [11]. In fact, insufficient consideration of all the biological process after implantation is one of the main reasons for the inconsistency between *in vitro* and *in vivo* results [12].

In the process of peri-implant bone healing, the bone-implant interaction *in vivo* is a dynamic process comprising different phases. After surgery, a cascade of biological events occurs that are impacted by multiple factors surrounding the artificial implants [13–16]. Prior to osteogenetic interactions, the host immune response is initiated within hours after implantation and macrophages play a central role in this early stage. Specifically, the recruited macrophages reaching the implant surface are activated into the M1 phenotype, followed by secretion of a small amount of inflammation-related cytokines that are required for bone healing. Nevertheless, if the pro-inflammatory M1 phenotype of macrophages persists for a long time, chronic inflammation can be triggered, resulting in fibrous encapsulation of implants and compromised bone-implant osseointegration [14,17]. In contrast, timely and efficient transformation of macrophages from the M1 to M2 phenotype not only eases acute inflammation with the aid of anti-inflammatory cytokines secretion, but also releases osteogenesis-related mediators to create a favorable osteoimmunomodulatory micro-environment to enhance ensuing bone regeneration [18]. Therefore, surface functionalization of PEEK implants should be designed more delicately with the consideration of immunomodulatory ability.

Following the early stage of positive immune regulation, peri-implant bone regeneration leads to bone formation and subsequent bone remodeling phases which are mainly orchestrated by two main cell types: osteoblasts and osteoclasts. In particular, osteoblasts are responsible for bone formation, whereas osteoclasts specialize in bone resorption. Successful peri-implant bone regeneration relies on the dynamic equilibrium between bone formation and bone resorption at the defect sites. In actuality, many old patients receiving implants suffer from degenerative diseases concurrently, especially osteoporosis. In osteoporotic patients, bone homeostasis is broken due to excessive bone resorption and insufficient bone formation [19–21], leading to the inferior quality and quantity of human bones. In these cases, accomplishing bone-implant osseointegration is more challenging compared to normal conditions.

By considering the various progressive biological events in bone-implant interactions after implantation and pathological characteristics of osteoporosis, a programmed degradable coating is designed and constructed on PEEK implant in this work. This coating can coordinate with the peri-implant biological response by initiating immune mediation in the early stage after implantation and ameliorating peri-implant bone regeneration thereafter. According to our design: (1) Poly(lactide-co-glycolide) (PLGA), a biodegradable and biocompatible polymer approved by FDA [22,23], is utilized as the coating material; (2) Alendronate (ALN), an effective therapeutic agent for preventing excessive bone resorption [24], is bound onto the osteo-inductive nano-hydroxyapatite (nHA) [25] to form nHA-ALN and homogeneously dispersed in the PLGA matrix; (3) Interleukin 4 (IL-4), a typical cytokine with anti-inflammatory effect [26,27], is grafted onto the outer surface of the PLGA@nHA-ALN hybrid coating with the aid of N_2 plasma immersion ion implantation (PIII) and subsequent immersion in IL-4 solution. Degradation of this gradient coating mediates the peri-implant biological response in sequence. As illustrated in Fig. 1, the initial burst of IL-4 dominates in the early post-implantation stage to create a favorable osteoimmunomodulatory micro-environment by timely switching of the peri-implant macrophages from the pro-inflammatory M1 phenotype to anti-inflammatory M2 phenotype.
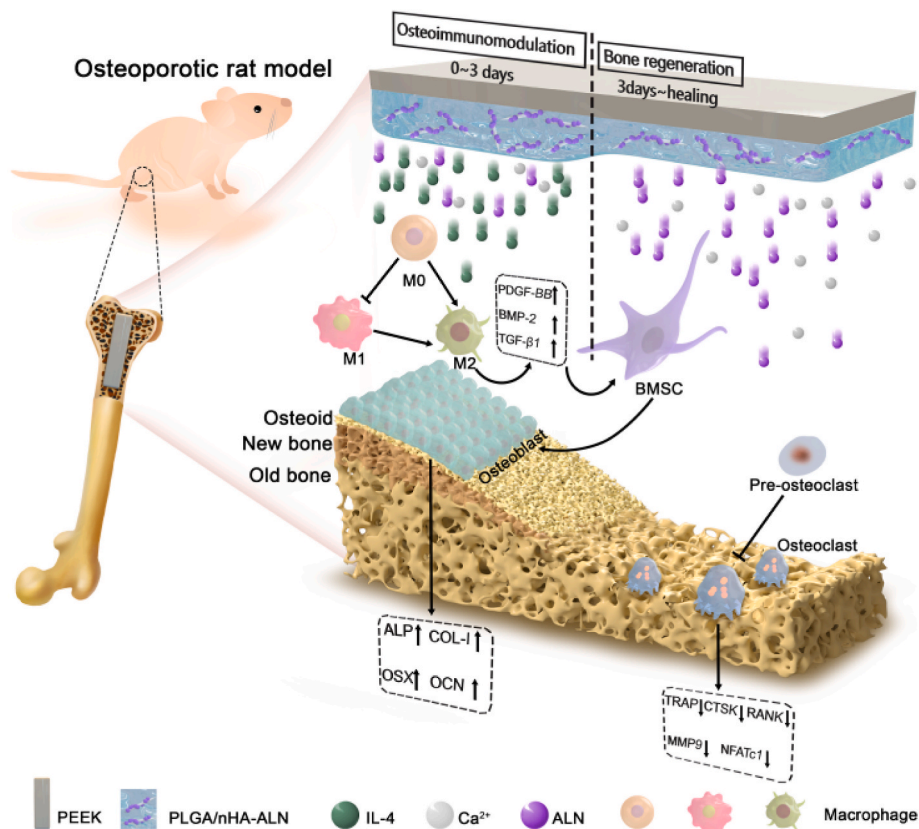

Fig. 1. Schematic illustration of the programmed surface on PEEK which enhances bone-implant osseointegration under osteoporotic conditions by creating a favorable osteoimmunomoduatory microenvironment in the early stage and facilitating bone regeneration thereafter.

Subsequently, slow and sustained release of ALN and Ca^{2+} in the next several weeks suppresses excessive bone resorption and enhances bone formation to restore peri-implant bone homeostasis and facilitate bone-implant integration under osteoporotic conditions. In this way, sequential regulation is achieved to match the dynamic process of bone regeneration. Our results reveal a new and clinically viable strategy to design advanced orthopedic implants, especially for osteoporotic patients.

2. Materials and methods

2.1. Materials

ALN, nHA, dexamethasone, ascorbic acid 2 phosphate, and β-glycerophosphate were purchased from Sigma-Aldrich (USA). PLGA (LA/GA 50:50, Mw 63000) was obtained from Daigang Biomaterials Inc. (Jinan, China) and recombinant Murine IL-4 and the receptor activator of nuclear factor kappa-B ligand (RANKL) were acquired from Peprotech (USA). The nHA-ALN was prepared in our laboratory, and the synthesis procedures and characterization results were presented in Fig. S1.

2.2. Fabrication of samples

Biomedical grade PEEK (GEHR Plastics Inc.) rods were cut into pieces with different dimensions of Φ15 × 2 mm and used for surface characterization, *in vitro* release assay, *in vitro* cell experiments, and *in vivo* subcutaneous implantation assay. Cylindrical samples (Φ2 × 7 mm) were prepared for *in vivo* rat femur intramedullary implantation. Samples were ground with abrasive paper progressively up to 3000 grits and ultrasonically cleaned in acetone, ethanol, and deionized water sequentially. The programmed surface was constructed on PEEK according to the schematic procedures illustrated in Fig. 2a. At first, the hybrid coating consisting of PLGA and nHA-ALN (10 wt%) was fabricated on PEEK by solvent evaporation. Briefly, PLGA was dissolved in dichloromethane to form a homogeneous solution and nHA-ALN was ultrasonically dispersed in a solution of ethanol and dichloromethane and added slowly to the PLGA solution. After stirring, the mixture was spread on PEEK, dried at room temperature until the hybrid coating was formed on sample surface. PEEK sample with hybrid coating was then subjected to N_2 PIII by applying a pulse frequency of 1000 Hz, pulse duration of 50 μs, and voltage of 2 kV for 60 min. Afterwards, the sample was incubated in the IL-4 solution (20 ng/ml) for 24 h for grafting, followed by rinsing with sterile phosphate buffered saline (PBS) three times to remove the loose IL-4. The experimental sample groups are
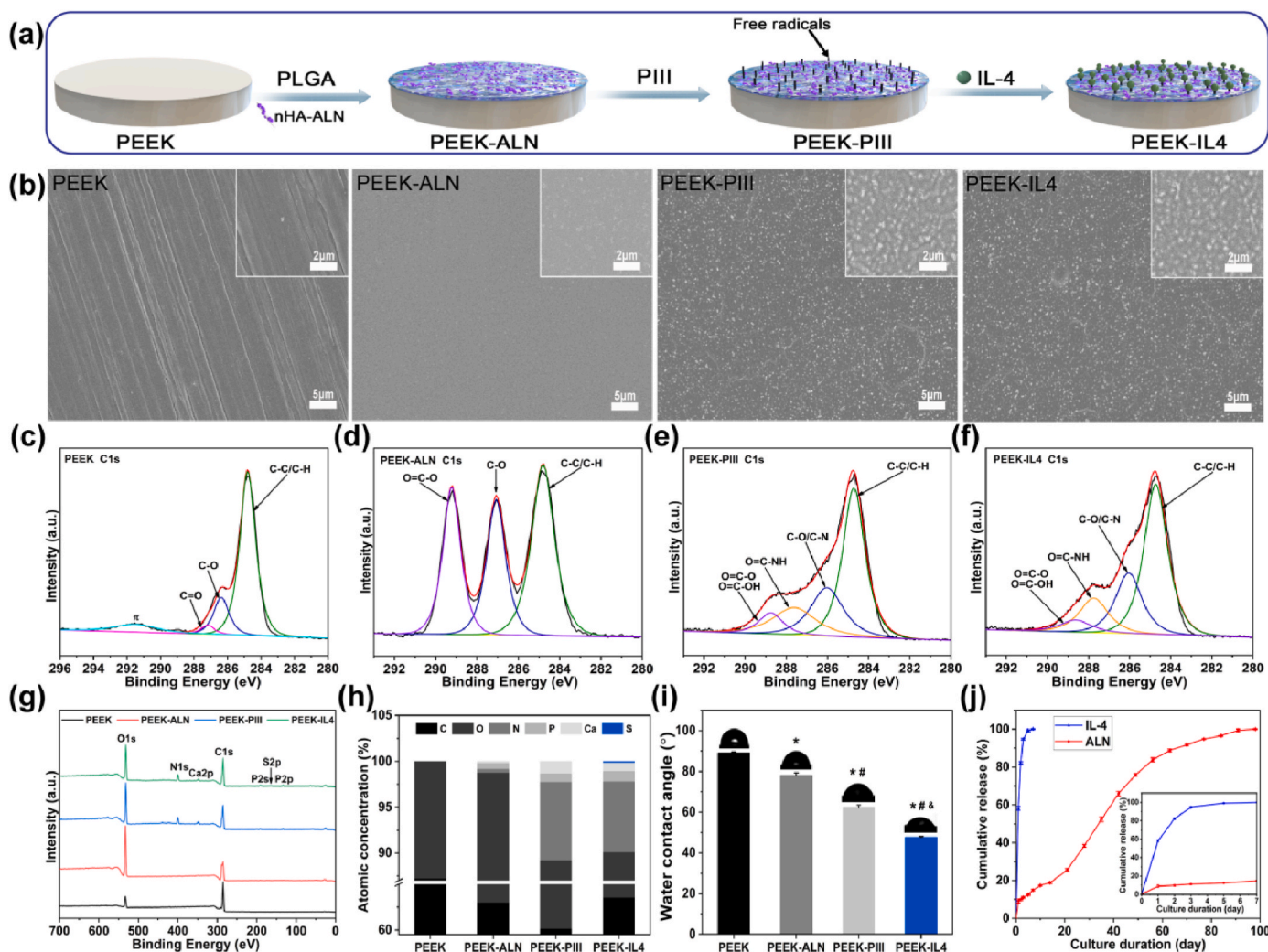
Fig. 2. Sample fabrication and characterization: (a) Schematic illustration of sample preparation; (b) Surface morphologies observed by FE-SEM; (c–f) High-resolution C1s spectra acquired from (c) PEEK, (d) PEEK-ALN, (e) PEEK-PIII, and (f) PEEK-IL4; (g) XPS survey spectra; (h) Atomic percentages determined by XPS; (i) Static water contact angles (n = 4 per group); (j) *In vitro* release profile of IL-4 and ALN from PEEK-IL4 incubated in the PBS solution at 37 °C (n = 6 per group). The inset presents the release profile in first 7 days. *$p < 0.05$ compared to PEEK, #$p < 0.05$ compared to PEEK-ALN, and &$p < 0.05$ compared to PEEK-PIII.

presented in Table 1.

2.3. Surface characterization

The surface morphology of samples was examined by field-emission scanning electron microscopy (FE-SEM, ZEISS SUPRA 55, Carl Zeiss, Germany) after sputter-coating with platinum. The surface hydrophilicity was measured with 4 μl of deionized water by the sessile drop method on a contact angle system (Attension Theta Flex, Biolin Scientific, Sweden) under ambient conditions. Four measurements were conducted on different samples of each group for the statistical accountability. The surface chemical composition and chemical state were determined by X-ray photoelectron spectroscopy (XPS, ESCALAB 250Xi, Thermo Fiser, England) with Al K_α radiation referenced to the C 1s peak at 284.8 eV.

2.4. In vitro release profile of IL-4, ALN and Ca^{2+}

To obtain release profiles of IL-4, ALN and Ca^{2+}, the PEEK-IL4 samples were placed in a 24-well plate containing 1 ml PBS per well and incubated at 37 °C. At prescribed time points, supernatant was collected and refilled with fresh PBS. The released IL-4 was quantified by the enzyme-linked immunosorbent assay (ELISA) kit (Valukine, R&D Systems, USA) following the manufacturer's instructions. The concentration of released ALN was determined by UV–visible spectrophotometry (UV-US, TU-1810, Pulse, China) at 293 nm according to the previously reported method [28]. The Ca^{2+} concentration was measured using a calcium colorimetric assay kit (Beyotime, China) according to the manufacturer's instructions.

2.5. Cell culture

Murine-derived macrophage cell line RAW264.7 and bone marrow mesenchymal stem cells isolated from osteoporosis rats (op-BMSCs) were used in this study. Both cells were cultured in Dulbecco's modified eagle medium (DMEM, Hyclone, USA) supplemented with 10% fetal bovine serum (FBS, Gibco, USA) and 1% penicillin/streptomycin (HyClone, USA) at 37 °C in humidified 5% CO_2 incubator. The op-BMSCs were isolated from femurs and tibias of Sprague-Dawley (SD) rats after ovariectomy three months under sterile conditions, and only 3 to 5 passages of op-BMSCs were used for the follow-up experiments. The experimental procedures were approved by the Ethics Committee for Animal Research, Shenzhen Institute of Advanced Technology, Chinese Academy of Sciences. For osteogenic induction, the culture medium was supplemented with 50 μg/ml ascorbic acid, 10 mM β-glycerophosphate and 100 nM dexamethasone.

2.6. The osteoimmunomodulatory properties of the programmed surface

2.6.1. Cell morphology and proliferation of RAW264.7 cells

The RAW264.7 cells were seeded on the specimens at a density of 2×10^4 cells/sample and cultured for 1, 3, and 5 days. Cell proliferation was determined by cell counting kit-8 (CCK-8) assay (Beyotime, China). At each time point, the culture medium was refreshed with 300 μl of serum-free medium containing 10% CCK-8. After incubation for 1.5 h at 37 °C, 100 μl of the supernatant were collected and the absorbance at a wavelength of 450 nm was measured by a microplate reader (Thermos

Table 1
Experimental sample groups in this study.

Groups	Treatment procedures
PEEK	Pristine PEEK
PEEK-ALN	PEEK + PLGA/nHA-ALN coating
PEEK-PIII	PEEK + PLGA/nHA-ALN coating + N_2 PIII
PEEK-IL4	PEEK + PLGA/nHA-ALN coating + N_2 PIII + IL-4 grafting

Fisher Scientific Inc., USA).

The morphology of the RAW264.7 cells was observed by FE-SEM. After culturing on the samples for 24 h, the cells were rinsed thrice with PBS and fixed with 2.5% glutaraldehyde, followed by dehydration in gradient ethanol (30%, 50%, 70%, 90%, 95% and 100%). The samples with cells were dried under atmospheric conditions, sputter-coated with platinum, and observed with FE-SEM.

2.6.2. The inflammatory response of RAW264.7 cells

To assess the inflammatory response, the expressions of immune, autophagy, and osteogenesis-related genes of RAW264.7 cells were evaluated by real-time polymerase chain reaction (RT-PCR). The RAW264.7 cells were seeded on each sample at a density of 3.0×10^4 cells/sample and cultured for 3 days. The total RNA was extracted from cultured cells using the TRIzol reagent (Life Technologies) and reversely transcribed into complementary DNA (cDNA) using a PrimeScript RT Master Mix kit (TaKaRa) following the manufacturer's instructions. Afterwards, RT-PCR (CFX 96, Bio-Rad, USA) was performed using a TransStart Green qPCR SuperMix UDG Kit (TransGen Biotech, China) as well as the forward and reverse primers as listed in Table S1. The expressions of immune-related genes (inflammatory cytokine genes: tumor necrosis factor α (TNF-α), interleukin 6 (IL-6), interleukin 1 beta (IL-1β), interleukin 4 (IL-4), and interleukin 10 (IL-10); macrophage-phenotype marker genes: cluster of differentiation 86 (CD86), C–C chemokine receptor type 7 (CCR7), inducible nitric oxide synthase (iNOS), cluster of differentiation 206 (CD206), cluster of differentiation 163 (CD163), and Arginase (Arg)), autophagy-related genes (autophagy-related gene 5 (ATG5), autophagy-related gene 7 (ATG7), microtubule-associated protein light chain 3B (LC3B), Beclin 1, and sequestosome-1(SQSTM1, also known as P62)), and osteogenesis-related genes (platelet derived growth factor BB (PDGF-BB), transforming growth factor beta 1 (TGF-β1), and bone morphogenetic protein 2 (BMP-2)) were quantitatively determined with β-actin serving as the house-keeping gene for normalization. The $2^{-\Delta\Delta Ct}$ method was employed to calculate the relative gene expression levels.

In a next step, the RAW264.7 cells were evaluated quantitatively for polarization by determining the percentage of iNOS-positive cells (M1 phenotype) and CD206-positive cells (M2 phenotype). After culturing for 3 days, the cells on different samples were harvested and collected into eppendorf tubes. Non-specific antigen was blocked by incubating with 1% BSA for 30 min. The cells were stained by the diluted flow direct-labeled iNOS and CD206 antibodies (eBioscience) for 30 min at room temperature in darkness. After washing thrice with PBS, the cells were tested by flow cytometry (CytoFLEXS, Beckman, USA) and the data were analyzed by the Flowjo.10.2 software. The RAW264.7 cells cultured on the different samples for 3 days were quantified for the release of cytokines TNF-α, IL-10 and TGF-β1 by ELISA using the commercial ELISA kits (Multisciences, China) according to the manufacturer's instructions.

2.6.3. Osteogenic differentiation of op-BMSCs in the macrophage-conditioned medium

The macrophage-conditioned medium was prepared by incubating RAW264.7 cells on the different samples. The medium after cell culturing was collected daily for three days and mixed with osteogenic induction medium with a ratio of 1:1. The conditioned medium of different groups without RAW264.7 cells was also prepared. After culturing op-BMSCs in a 24-well plate for 2 days, the medium was replaced with the conditioned medium every 2 or 3 days up to 7 days.

After conditioned culturing for 3 and 7 days, the op-BMSCs in different groups were treated with the cell lysis buffer (Beyotime, China). The alkaline phosphatase (ALP) activity and total intracellular protein in the cell lysis were quantitatively determined by the ALP Assay Kit (Beyotime, China) and BCA Protein Assay Kit (Beyotime, China), respectively per the manufacturer's protocols. The results of ALP activity were normalized to the total protein content and described as

nmol/min/mg protein.

The degree of extracellular matrix (ECM) mineralization was evaluated by alizarin red staining. After conditioned culturing for 7 days, cells on different samples were fixed in 75% ethanol for 1 h and stained with 1% alizarin red S solution (pH 4.2, Solarbio, China) for 10 min at room temperature. The unbound stain was removed by flushing with distilled water and the bound stain was eluted with 500 μl of cetylpyridinium chloride in 10 mM sodium phosphate (10%, pH 7.0). In the quantitative analysis, the eluted solution in each group was tested for the absorbance at 620 nm using a microplate reader.

2.7. Osteogenic properties of the programmed surface

2.7.1. Cell viability of op-BMSCs

The op-BMSCs were seeded on the different samples at a density of 1.5×10^4 cells/sample. After incubation for 4 and 24 h, the morphology of op-BMSCs was observed by FE-SEM. Cell proliferation was evaluated after culturing op-BMSCs on different samples for 1, 3 and 5 days. At each time point, CCK-8 assay was performed as described above. The op-BMSCs cultured on different samples for 3 days were also evaluated by live/dead cell staining. Calcein-AM and propidium iodide (Beyotime, China) were utilized to stain the live cells in green and dead cells in red, respectively. The stained cells were examined by fluorescent microscopy (Eclipse CI, Nikon, Japan).

The ALP activity and ECM mineralization of op-BMSCs cultured on different samples were evaluated after osteogenic induction for 7 and 14 days. These assays were performed using the protocols described in Section 2.6.3. At the same time points, the gene expressions of ALP, type I collagen (COL-I), osterix (OSX), and osteocalcin (OCN) were analyzed by RT-PCR as described above. The forward and reverse primers are listed in Table S1.

2.8. Osteoclastic properties of the programmed surface

RAW264.7 cells were inoculated on each sample at a density of 5×10^4 cells/sample and DMEM complete medium containing RANKL (50 ng/ml) was employed to induce the differentiation of RAW264.7 cells to osteoclast-like cells. After culturing for 9 days, the cells on each sample were lysed and evaluated for the tartrate-resistant acid phosphatase (TRAP) activity and total intracellular protein using a commercial TRAP Assay Kit (Beyotime, China) and BCA Protein Assay Kit, respectively per the manufacturer's protocols. The TRAP activity was normalized to the total protein content and described as nmol/min/mg protein.

At the same time point, the expressions of osteoclastogenesis and autophagy-related genes were analyzed by RT-PCR following the protocols described in section 2.6.3. The osteoclastogenesis-related genes included TRAP, cathepsin K (CTSK), matrix metalloproteinase-9 (MMP9), nuclear factor of activated T-cells cytoplasmic 1 (NFATc1), and receptor activator of nuclear factor kappa-B (RANK) and the autophagy-related genes included ATG5, ATG7, LC3B, Beclin1, and P62. The forward and reverse primers are listed in Table S1.

2.9. In vivo assessments

All the animal experiments and protocols were approved by the Ethics Committee for Animal Research, Shenzhen Institute of Advanced Technology, Chinese Academy of Sciences (Certificate number: SIAT-IACUC-210223-YYS-ZYY-A0969-03).

2.9.1. Immunomodulatory evaluation after subcutaneous implantation

The immunomodulatory ability was evaluated after subcutaneous implantation, and 12-weeks-old male SD rats with a body weight of 200–300 g were used in this *in vivo* study. After general anesthesia by intraperitoneal injection of 2% pentobarbital (2 ml/kg), the back of rats was shaved and sterilized using povidone iodine. A longitudinal incision was created and a subcutaneous pocket was dissected. The samples were

implanted into the pockets and the incisions were carefully closed. After 3 and 7 days post-operation, the rats were sacrificed and the specimens with surrounding tissues were harvested. The biopsy samples were fixed in paraformaldehyde, embedded in paraffin, sectioned, and observed after hematoxylin and eosin (H&E) (Servicebio, China) staining. Immunofluorescence staining was performed to examine the macrophage polarization around implants using the primary antibodies of iNOS (M1 marker, Servicebio, china) and CD163 (M2 marker, Servicebio, china) as well as the corresponding secondary antibodies (Servicebio, china). Meanwhile, the nuclei were stained blue with 4′,6-diamidino-2-phenylindole (DAPI, Servicebio, China) and all the stained sections were examined by fluorescent microscopy. Image-Pro Plus software was employed to analyze the thickness of the fibrous layer as well as the ratio of iNOS-positive/CD163-positive cells.

2.9.2. Osseointegration evaluation after femoral implantation in osteoporotic rats

Twelve aged female SD rats (20-month-old) with osteoporosis were randomly assigned into three groups (PEEK group, PEEK-ALN group, and PEEK-IL4 group). After general anesthesia by intraperitoneal injection of 2% pentobarbital (2 ml/kg), a 10 mm longitudinal incision was made along the lateral side of the extensor mechanism around the knee joint. With the knee in flexion, a cylindrical defect (Φ 2 × 7 mm) was drilled at the intercondylar notch of the distal femur (parallel to the long axis of the femur). The implants with different surfaces were inserted into the defects and the wounds were closed carefully. The surgery procedures of implanting different samples into the bone defects are shown in Fig. S2. The different samples were randomly implanted in the bilateral femurs of experimental rats for symmetry. After 2 weeks post-implantation, alizarin red (30 mg/kg) was intraperitoneally administered in the rats to label the peri-implant new bone formation and mineralization.

The rats were sacrificed 4 weeks post-operation and the femurs containing implants were harvested and fixed in paraformaldehyde. Peri-implant new bone formation was evaluated by micro-computed tomography (micro-CT) (SkyScan 1176, Bruker, Germany) and the 3D images were reconstructed by the CTvol program (Skyscan). A hollow cylinder with a thickness of 180 μm from the implant surface and a length of 5 mm of the implant (1 mm each away from the implant ends) was defined as the volume of interest. Qualitative analysis of bone mineral density (BMD), bone volume/total volume (BV/TV), trabecular number (Tb.N), and trabecular separation (Tb.Sp) was conducted by 3D bone morphometric analysis. Subsequently, the fixed femurs were embedded in poly (methyl methacrylate), and cut into sections using the Exakt system (310CP, Exakt, Germany). The sections were ground and polished to a final thickness of about 50 μm. Fluorescent observation was performed on a confocal laser microscope (TCS SP8, Leica, Germany) with excitation/emission wavelengths at 543/620 nm for alizarin red. The slices were further processed by toluidine blue staining to visualize the bone-implant interfaces. Finally, the femurs after removal of implants were decalcified, embedded in paraffin, sectioned into slices, and processed by H&E and TRAP (Sigma-Aldrich) staining according to the standard protocols.

2.10. Statistical analysis

All the experiments were performed at least in triplicate, and the results were shown as mean ± standard deviation (SD). The one-way analysis of variance (ANOVA) and least significant difference (LSD) post hoc test were performed to determine the statistical significance. A difference at *$P < 0.05$ was considered to be statistically significant.

3. Results and discussion

3.1. Sample characterization

The PEEK specimens with different surfaces are prepared as shown in Fig. 2a. The degradable PLGA@nHA-ALN coating is deposited on PEEK and then N_2 PIII is conducted to activate the surface. During N_2 PIII treatment, energetic nitrogen ions are implanted into the hybrid coating, and thus abundant free radicals are generated in ion-implanted region underneath the surface. A substantial amount of the free radicals can continuously migrate to the surface without being quenched and react with environmental molecules. By taking advantage of this unique mechanism, simple incubation of the PIII-treated samples in the IL-4 solution enables grafting of IL-4 without using chemical linkers [29]. FE-SEM discloses that the pristine PEEK surface is relatively flat and smooth with only a few scratches resulting from sandpaper grinding, as shown in Fig. 2b. After deposition of the PLGA@nHA-ALN coating, PEEK-ALN has a homogeneous and flat surface without scratches, indicating that nHA-ALN is evenly distributed in the PLGA. Compared with PEEK-ALN, the surface topography of PEEK-PIII and PEEK-IL4 is strikingly different, indicating that the energetic plasma etches the outer surface of the hybrid coating to expose the underlying nHA-ALN. The cross-sectional FE-SEM image in Fig. S3 shows that the coating is about 13 μm thick and bonds well with the PEEK substrate.

XPS is employed to determine the chemical states of the different surfaces. The high-resolution C 1s spectra illustrate the changes in the surface chemical states after each step (Fig. 2c–f). Compared to the C 1s spectrum of pristine PEEK (Fig. 2c), the characteristic peaks of PLGA in the C 1s spectrum arise from PEEK-ALN (Fig. 2d) thereby corroborating successful fabrication of the PLGA@nHA-ALN coating. In the N_2 PIII treatment, energetic nitrogen ions are implanted into the hybrid coating and new chemical bonds like C–N at 286.3 eV and O=C–NH at 287.8 eV emerge from the PEEK-PIII surface (Fig. 2e). The bulge at 287.8 eV in the C 1s spectrum of PEEK-IL4 (Fig. 2f) can be ascribed to the abundant O=C–NH group in IL-4. The other chemical changes are observed from the high-resolution Ca 2p, P 2p, N 1s, and S 2p spectra as shown in Fig. S4. In general, the peaks of Ca 2p, P 2p, and N 1s are accentuated on PEEK-PIII, and the S 2p peak originating from IL-4 can only be detected from PEEK-IL4. Fig. 2g shows the survey XPS spectra of the different samples and the corresponding atomic percentages are presented in Fig. 2h. Only C and O are dominant on the pristine PEEK sample, while Ca, P, and N are detected from the surface of PEEK-ALN. In comparison with PEEK-ALN, PEEK-PIII and PEEK-IL4 show larger atomic percentages of Ca, P, and N. It is probably due to the plasma etching effect of N_2 PIII subsequently exposing more nHA-ALN on the outer surface and some N-containing groups are also introduced by the plasma. A trace amount of S is also detected from PEEK-IL4 to confirm the successful grafting of IL-4.

The surface hydrophilicity of the specimens is evaluated by the static contact angle measurement. As shown in Fig. 2i, the water contact angle on the pristine PEEK is 89.1° and decreases to 78.1° after deposition of PLGA@nHA-ALN coating. The surface of PEEK-PIII is more hydrophilic showing a water contact angle of 62.3°. This is because PIII exposes some nHA-ALN in the coating and also introduces hydrophilic N-containing groups as shown by XPS. The water contact angle on PEEK-IL4 is as low as 47.7° corroborating good hydrophilicity of the surface grafted IL-4.

3.2. In vitro release of IL-4, ALN and Ca^{2+}

With regard to the gradient of surface coating, the release behaviors of IL-4, ALN, and Ca^{2+} from PEEK-IL4 sample are evaluated by PBS incubation. As shown in Fig. 2j, rapid release of IL-4 (more than 90% of the total grafted amount) is detected during the initial 3 days. However, the cumulative release of ALN shows a different profile. After incubation for 1 day, burst release of about 9% of the total encapsulated ALN is

detected and then sustained release of ALN occurs for up to 98 days. Release of Ca^{2+} from PEEK-IL4 shows a similar curve as ALN (Fig. S5). These results meet our anticipation of the programmed surface that IL-4 grafted on the outer surface dominates release in the first few days, while the hybrid coating with good degradability serves as a reservoir to sustain subsequent release of ALN and Ca^{2+} in the next several weeks. In this way, IL-4 contributes to the immunomodulatory effects on the programmed surface in the early stage after implantation, and thereafter ALN and Ca^{2+} inhibit osteoclastogenesis and promote osteogenesis under osteoporotic conditions.

3.3. In vitro osteoimmunomodulatory properties

3.3.1. Inflammatory response of RAW264.7 cells

After implantation, the artificial implants are recognized as foreign matters by the host immune system. In response to the physicochemical properties of the implant surface, immune cells are recruited to the implant surface to alter the local microenvironment by switching phenotypes [14,15]. Among the various immune cells, macrophages play a crucial role in the host immune response, which mediates subsequent bone healing and ultimately determines the fate of implants in vivo [14, 30]. Therefore, RAW264.7 macrophages are cultured on our samples to investigate the early inflammatory response.

After incubation for 24 h, cell morphology is examined by FE-SEM as shown in Fig. 3a. The RAW264.7 cells cultured on PEEK and PEEK-ALN have a spindle appearance while pseudopodia are more obvious on PEEK-ALN. In comparison, macrophages attach better on PEEK-PIII and PEEK-IL4 by presenting an extended morphology with more pseudopodia. Fig. 3b shows the proliferation of RAW264.7 cells after culturing for 1, 3, and 5 days. Compared to the PEEK control group, all the modified surfaces inhibit proliferation of macrophages on the 3rd and 5th day and no significant difference in cell proliferation is observed from PEEK-ALN, PEEK-PIII, and PEEK-IL4.

To evaluate polarization of macrophages, the M1-and M2-related gene expression is determined by RT-PCR after culturing RAW264.7 cells on different samples for 3 days. The results are presented as heat maps in Fig. 3c and d and the original quantitative data are shown in Fig. S6. The M1 phenotype markers CCR7, CD86, and iNOS, and pro-inflammatory cytokines such as TNF-α, IL-6, and IL-1β are referred to as the M1-related genes. The M2 phenotype markers CD163, CD206, and Arg, and anti-inflammatory cytokines like IL-4 and IL-10 are referred to as the M2-related genes. Fig. 3c shows that all the M1-related genes are down-regulated after culturing the macrophages on the modified samples and the lowest expression is detected from PEEK-IL4. On the contrary, the expression of M2-related genes shows a reverse trend that the highest expression is observed from PEEK-IL4. Polarization of macrophages is also confirmed by flow cytometry. As shown in Fig. 3e and Fig. S7, the proportion of iNOS-positive cells (M1 phenotype) decreases from 57% on PEEK to 17% on PEEK-IL4. Meanwhile, the CD206-positive cells (M2 phenotype) increase from 27% on PEEK to 69% on PEEK-IL4 (Fig. 3f and Fig. S7). Moreover, the levels of osteogenic-related genes (PDGF-BB, TGF-β1, and BMP-2) are elevated after culturing macrophages on the various samples for 3 days and the highest expression is detected from PEEK-IL4 (Fig. 3g).

Secretion of extracellular cytokines is monitored by the ELISA. As expected, the release trends of pro-inflammatory cytokine TNF-α (Fig. 3h), anti-inflammatory cytokine IL-10 (Fig. 3i), and osteogenic cytokine TGF-β1 (Fig. 3j) are consistent with the gene expressions. The results clearly show that the modified samples, especially PEEK-IL4, possess the immunomodulatory ability to inhibit pro-inflammatory M1 polarization and promote the anti-inflammatory and pro-healing M2 polarization of macrophages. Therefore, PEEK-IL4 has the greatest potential to generate a favorable immune microenvironment for facilitating bone regeneration. It is recognized that the surface properties of implants affect the peri-implant immune response [14,31]. As a classic M2-polarizing cytokine, IL-4 is grafted onto the sample surface and its
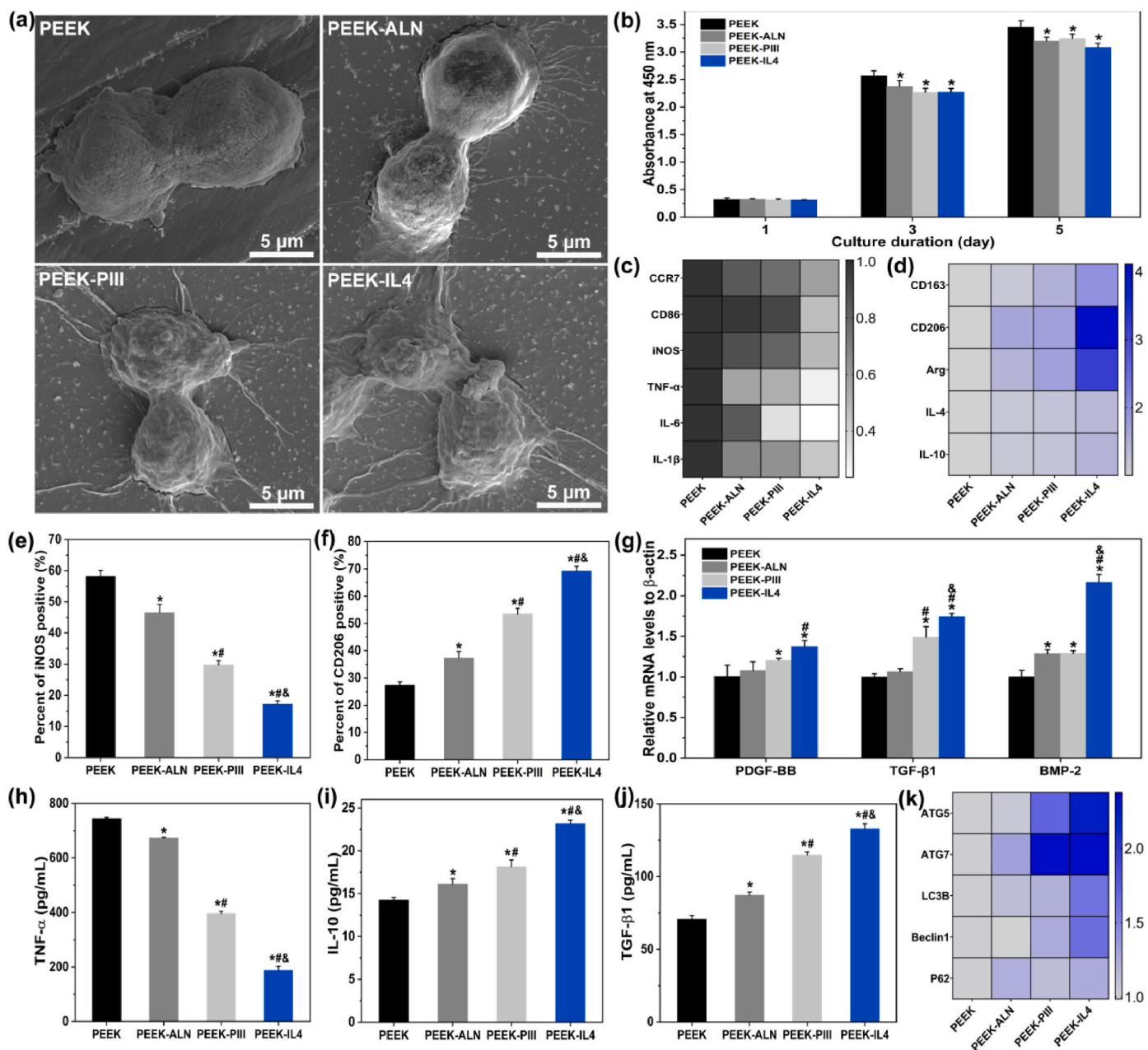
Fig. 3. Inflammatory response of RAW264.7 cells cultured on different samples: (a) Cell morphology after culturing for 24 h; (b) Cell proliferation after culturing for 1, 3, and 5 days (n = 4 per group); (c) Heat map showing the expression of M1 markers (CCR7, CD86, and iNOS) and pro-inflammatory genes (TNF-α, IL-6, and IL-1β) after incubation for 3 days (n = 4 per group); (d) Heat map showing the expression of M2 markers (CD163, CD206, and Arg) and anti-inflammatory genes (IL-4 and IL-10) after incubation for 3 days (n = 4 per group); (e–f) Percentage of (e) iNOS-positive macrophages (M1 phenotype) and (f) CD206-positive macrophages (M2 phenotype) after incubation for 3 days (n = 3 per group); (g) Expression of osteogenic-related genes (PDGF-BB, TGF-β1, and BMP-2) after incubation for 3 days (n = 4 per group); (h–j) Secretion of (h) TNF-α, (i) IL-10, and (j) TGF-β1 after incubation for 3 days (n = 4 per group); (i) Heat map showing the expression of autophagy-related genes (ATG5, ATG7, LC3B, Beclin1, and P62) after incubation for 3 days (n = 4 per group). $*p < 0.05$ compared to PEEK, $\#p < 0.05$ compared to PEEK-ALN, $\&p < 0.05$ compared to PEEK-PIII.

release dominates in the first several days [26,32,33]. In addition, both the HA-modified surfaces and ALN released from biomaterials have been reported to down-regulate secretion of pro-inflammatory cytokines from macrophages [34,35]. In this respect, the programmed surface on PEEK-IL4 shows the optimal immunomodulatory capability due to the synergetic effects rendered by IL-4 and nHA-ALN.

Autophagy is a cellular waste disposal process that plays an important role in maintaining intracellular homeostasis and actively participates in immune-surveillance [36]. Autophagy can suppress the activation of inflammasome as an indicator of the anti-inflammatory response [36]. Hence, the effects of autophagy are evaluated by

RT-PCR. As shown in Fig. 3k and Fig. S8, the expressions of autophagy-related genes (ATG5, ATG7, LC3B, Beclin 1, and P62) are up-regulated on the modified samples, especially PEEK-IL4. The favorable immunomodulatory ability of PEEK-IL4 may thus be associated with the activation of autophagy.

3.3.2. Osteogenic differentiation of op-BMSCs in the conditioned medium

To determine the immunomodulatory effects of the modified samples on osteogenesis of op-BMSCs, the conditioned medium with (+) or without (−) seeding of macrophages is collected daily and supplied to op-BMSCs every 2 or 3 days according to the protocols shown in Fig. 4a.
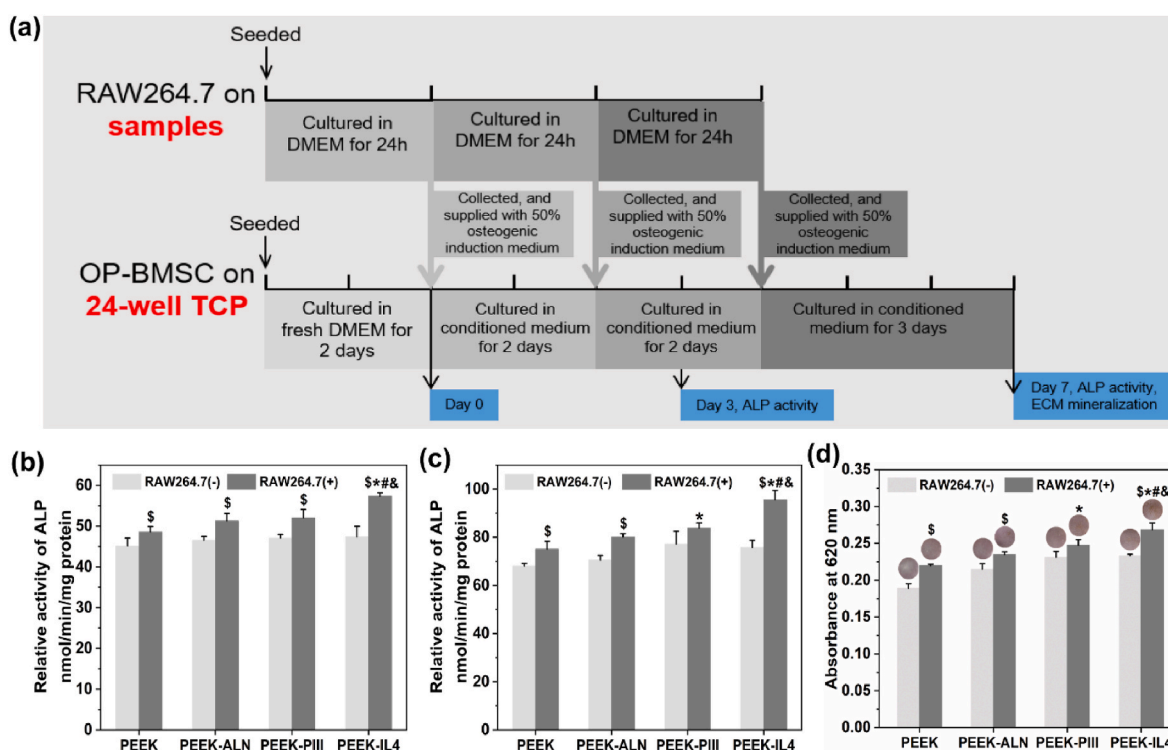
Fig. 4. Osteogenic differentiation of op-BMSCs in the conditioned medium: (a) Experimental design of the conditioned culture and analysis; (b–c) ALP activity of op-BMSCs cultured in the RAW264.7 (+) or RAW264.7 (−) conditioned medium of different groups for (b) 3 and (c) 7 days (n = 3 per group); (d) Quantitative results and corresponding images of ECM mineralization of op-BMSCs cultured in the RAW264.7 (+) or RAW264.7 (−) conditioned medium of different groups for 7 days (n = 3 per group). $^{\$}p < 0.05$ by comparing RAW 264.7 (+) to RAW264.7 (−) in each group, $^{*}p < 0.05$ compared to RAW264.7 (+) in PEEK, $^{\#}p < 0.05$ compared to RAW264.7 (+) in PEEK-ALN, $^{\&}p < 0.05$ compared to RAW264.7 (+) in PEEK-PIII.

The ALP activity, an early marker of osteogenic differentiation, is evaluated after culturing op-BMSCs for 3 and 7 days. As shown in Fig. 4b and c, the ALP activity of op-BMSCs is up-regulated by the RAW264.7 (+) condition medium compared to the parallel RAW264.7 (−) groups. The RAW264.7 (+) conditioned medium collected from PEEK-IL4 shows the highest ALP activity of op-BMSCs at both time points. In addition to the ALP activity, the results of ECM mineralization after culturing op-BMSCs for 7 days show a similar trend as presented in Fig. 4d. Therefore, the immune micro-environments created by the macrophages cultured on the modified samples, especially PEEK-IL4, are favorable to the osteogenic differentiation of op-BMSCs, hence validating that PEEK-IL4 has the best osteoimmunomodulatory effects. As aforementioned, the programmed surface on PEEK-IL4 prompts an efficient and timely switch of macrophages from the M1 to M2 phenotype, and the M2 macrophages can secret a series of osteogenic cytokines such as PDGF-BB, TGF-β1 and BMP-2 to facilitate the osteogenesis of op-BMSCs. TGF-β1 and BMP-2 are the pivotal members of the TGF-β superfamily that can promote osteogenesis and angiogenesis through their receptors [37–39], and PDGF-BB not only promotes vessel maturation, but also stimulates bone regeneration during the healing process [40–42]. Therefore, up-regulated secretion of osteogenic cytokines from macrophages after incubation is responsible for the osteoimmunomodulatory capacity of PEEK-IL4 to some extent.

3.4. In vitro osteogenesis and osteoclastogenesis

The op-BMSCs are used for the *in vitro* evaluation of osteogenesis and the cell morphology, cell proliferation, ALP activity, osteogenic gene expression, as well as ECM mineralization are investigated. It is well known that initial adhesion and spreading of cells on biomaterials are prerequisite to proliferation and differentiation [43]. As shown in Fig. 5a, spindle cells with an elongated shape are observed from PEEK

after incubation for 4 h indicative of poor cell adhesion. In contrast, the cells cultured on PEEK-ALN are more extended, whereas those on PEEK-PIII and PEEK-IL4 exhibit a flat morphology with apparent filopodia and lamellipodia. After incubation for 24 h, the extension of op-BMSCs on PEEK is limited but the cells on PEEK-ALN, PEEK-PIII, and PEEK-IL4 spread out extensively. It is possible that nHA-ALN exposed on the outer surface of PLGA@nHA-ALN coating after N$_2$ PIII provides more anchoring sites for cell attachment [44]. Bone mesenchymal stem cells are the precursor cells of osteoblasts and their proliferation is fundamental to bone regeneration *in vivo* [45]. Herein, time-dependent proliferation of op-BMSCs on different samples is assessed by CCK-8 assay as shown in Fig. 5b. The viability of op-BMSCs on PEEK-IL4 is significantly higher than that of the other 3 groups beginning with the first day. Noteworthily, proliferation of op-BMSCs on the samples is different from that of RAW264.7 cells. This can be ascribed to different response of cells to the effector molecules as reported previously [35,46]. The live/dead staining results (Fig. S9) confirm that PEEK-IL4 has better compatibility to op-BMSCs than the other samples.

After osteogenic induction for 7 and 14 days, the op-BMSCs in different groups are examined for the expression of osteogenic genes (ALP, COL-I, OSX, and OCN) by RT-PCR. The results are presented as heat maps in Fig. 5c and the original quantitative data are provided in Fig. S10. In general, the PEEK-IL4 group shows the highest levels of all the osteogenic genes at both time points. To verify the osteogenic performance of different samples, the ALP activity and ECM mineralization of cultured op-BMSCs are evaluated at the same time points. As shown in Fig. 5d, the ALP activity of op-BMSCs is up-regulated on the modified samples and the highest levels are observed from PEEK-IL4. Meanwhile, the quantitative results of ECM mineralization exhibit the same trend of PEEK-IL4 > PEEK-PIII > PEEK-ALN > PEEK (Fig. 5e), thus corroborating that PEEK-IL4 is more desirable than the other samples for boosting *in vitro* osteogenesis of op-BMSCs.
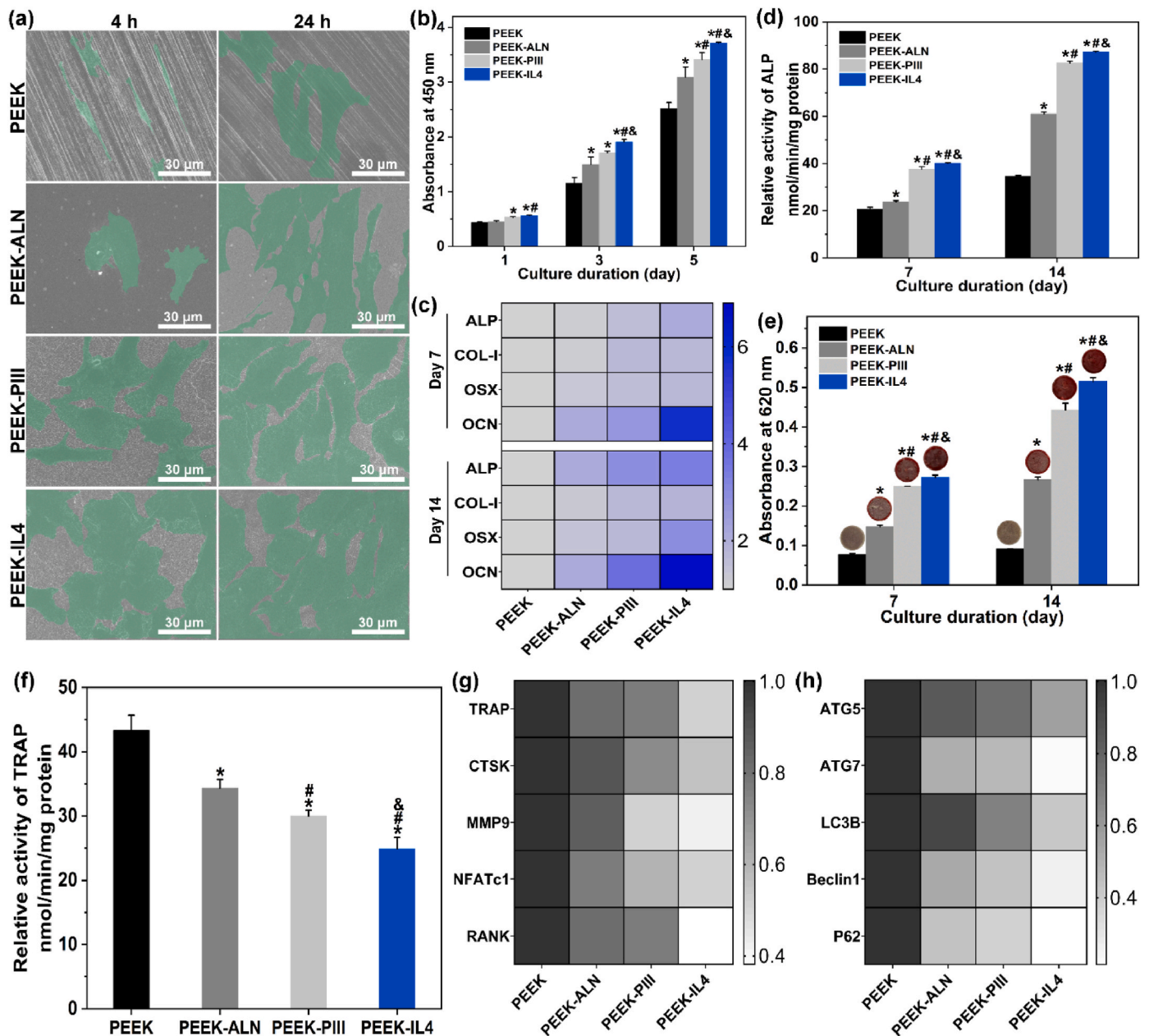
Fig. 5. Osteogenesis of op-BMSCs and osteoclastogenesis of RANKL-induced RAW264.7 cells cultured on the different samples: (a) Morphology of op-BMSCs after culturing for 4 and 24 h; (b) Proliferation of op-BMSCs after culturing for 1, 3 and 5 days (n = 4 per group); (c) Heat map showing the expression of osteogenesis-related genes (ALP, COL-I, OSX, and OCN) of op-BMSCs after osteogenic induction for 7 and 14 days (n = 4 per group); (d) ALP activity of op-BMSCs after osteogenic induction for 7 and 14 days (n = 3 per group); (e) Quantitative results and corresponding images of ECM mineralization of op-BMSCs after osteogenic induction for 7 and 14 days (n = 3 per group); (f) TRAP activity of RAW264.7 cells after induction by RANKL for 9 days (n = 4 per group); (g–h) Heat map showing the expression of (g) osteoclastogenesis-related genes (TRAP, CTSK, MMP9, NFATc1, and RANK) and (h) autophagy-related genes (ATG5, ATG7, LC3B, Beclin1 and P62) of RAW264.7 cells after induction by RANKL for 9 days (n = 4 per group). $*p < 0.05$ compared to PEEK, $^{\#}p < 0.05$ compared to PEEK-ALN, $^{\&}p < 0.05$ compared to PEEK-PIII.

Osteoporosis is characterized by excessive osteoclastogenesis that aggravates bone loss [47–49]. Therefore, proper reduction of osteoclast differentiation can rebalance the bone metabolism to favor bone regeneration, thus ameliorating bone-implant osseointegration under osteoporotic conditions. In this regard, RAW264.7 macrophages are induced by the RANKL to form osteoclasts and then examined for osteoclastogenesis after incubation on the different samples for 9 days. As shown in Fig. 5f, the TRAP activity of the cells in different groups follows the trend of PEEK > PEEK-ALN > PEEK-PIII > PEEK-IL4, indicating that the modified samples especially PEEK-IL4 provide the anti-osteoclastic activity. To further investigate the effects on osteoclastogenesis, the expression levels of genes including TRAP, CTSK,

MMP9, NFATc1, and RANK are evaluated. Fig. 5g and Fig. S11a show that the expressions of osteoclastogenesis-related genes are all the lowest in the PEEK-IL4 group. Evidently, the PEEK-IL4 sample with programmed surface shows the best capability of *anti*-osteoclastogenesis among the 4 groups.

With regard to the osteogenic and anti-osteoclastic functions of PEEK-IL4, there are synergistic effects rendered by IL-4, ALN and Ca²⁺ in our design. Particularly, cytokine IL-4 can serve as a chemotactic factor to recruit osteoblasts and play an important role in bone remodeling [50–52]. Recent studies have demonstrated that IL-4 can also inhibit the formation of osteoclasts from their precursor cells and even suppress the resorptive capacity of mature osteoclasts [53,54]. ALN is recognized to

be an effective anti-osteoporosis drug which can promote proliferation and osteogenic differentiation of osteoblasts and inhibit maturation of osteoclasts by disrupting the mevalonate pathway [24,48,55,56]. A sustained release of Ca^{2+} can ameliorate proliferation and osteogenic differentiation of osteoblasts as reported previously [44,57].

Autophagy is closely related to bone resorption [36,58,59]. Activation of autophagy has been reported to be involved in RANKL-induced differentiation of osteoclasts and therefore, attenuation of autophagy is proposed to suppress osteoclastogenesis. The expression of autophagy-related genes is further evaluated after inducing RAW264.7 cells on different samples with RANKL for 9 days. As shown in Fig. 5h and Fig. S11b, all the autophagy-related genes including ATG5, ATG7, LC3B, Beclin1 and P62 are down-regulated on the modified samples and the lowest expression is detected in the PEEK-IL4 group. P62 is an important protein bridging autophagy and RANKL-induced osteoclastogenesis, and knockdown of P62 can inhibit osteoclastic differentiation of macrophages [59]. The autophagic proteins ATG5, ATG7, and LC3 also participate in generating the mature ruffled border and releasing H^+ and CTSK to resorb bone [36]. Therefore, our results suggest that the modified samples, especially PEEK-IL4, suppress osteoclastogenesis by blocking autophagy.

3.5. Immunomodulatory evaluation in vivo

After surgery, inflammatory cell infiltration is a typical foreign body reaction of extraneous implants. In this early stage, excessive inflammatory reaction will lead to a fibrous layer surrounding the implant in vivo [60,61]. To study whether the programmed surface can ease the acute inflammatory response, PEEK, PEEK-ALN, and PEEK-IL4 are subcutaneously implanted into the back of SD rats for 3 and 7 days. At both time points, the inflammatory status of the peri-implant tissues is analyzed by H&E staining and immunofluorescence analysis. As shown in Fig. 6a and b, the fibrous layer after implantation of PEEK-IL4 is markedly thinner than those surrounding the PEEK and PEEK-ALN implants. Further immunofluorescence analysis demonstrates that the ratio of M1 macrophages ($iNOS^+$) to M2 macrophages ($CD163^+$) is the smallest in the PEEK-IL4 group (Fig. 6c–d and Fig. S12). Collectively, the in vivo results after subcutaneous implantation are in line with the aforementioned in vitro results showing that the programmed surface on PEEK-IL4 can effectively relieve the inflammatory response in the early stage after implantation.

3.6. In vivo bone regeneration in osteoporotic rats

To evaluate in vivo osseointegration under osteoporotic conditions, aged rats with osteoporosis are utilized as the animal model to create femur defects for implantation. As shown by the micro-CT results (Fig. S13), the aged rats suffer from striking bone loss compared to normal adult rats, illustrating successful establishment of the osteoporotic animal model. The untreated and modified samples are implanted separately into the femur defects of osteoporotic rats and in vivo bone regeneration is monitored after 4 weeks. Fig. 7a depicts the reconstructed transverse, coronal, and 3D micro-CT images of the peri-implant bone tissues in different groups. Correspondingly, the quantitative results of osteogenesis-related parameters including the BMD, BV/TV, Tb.N, and Tb.Sp are analyzed and shown in Fig. 7b–e. The results obtained from the PEEK-IL4 group are superior, followed by PEEK-ALN group and the PEEK group is inferior, indicating that quantity and quality of newly formed bone surrounding PEEK-IL4 implant with a programmed surface are significantly improved. The osteogenesis
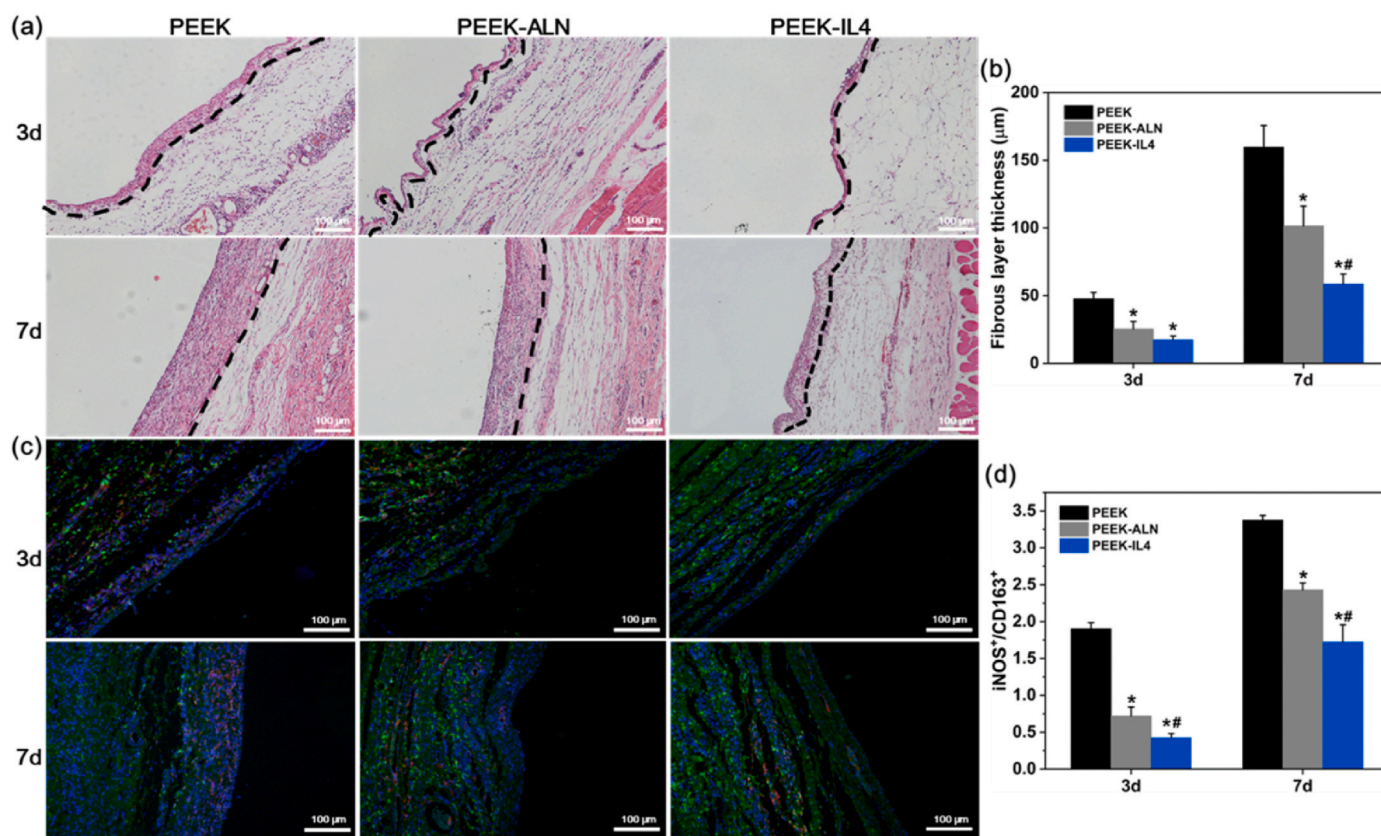

Fig. 6. In vivo immunomodulatory efforts: (a) H&E staining of the peri-implant tissues after subcutaneous implantation for 3 and 7 days with the fibrous layers marked by dashed lines; (b) Thickness of the fibrous layers around the implants (n = 6 per group); (c) Immunofluorescent staining of the peri-implant tissues after subcutaneous implantation for 3 and 7 days: red (iNOS, M1 marker), green (CD163, M2 marker) and blue (nuclei); (d) Ratios of iNOS-positive cells to CD163-positive cells in the peri-implant tissues (n = 6 per group). *$p < 0.05$ compared to PEEK, #$p < 0.05$ compared to PEEK-ALN.
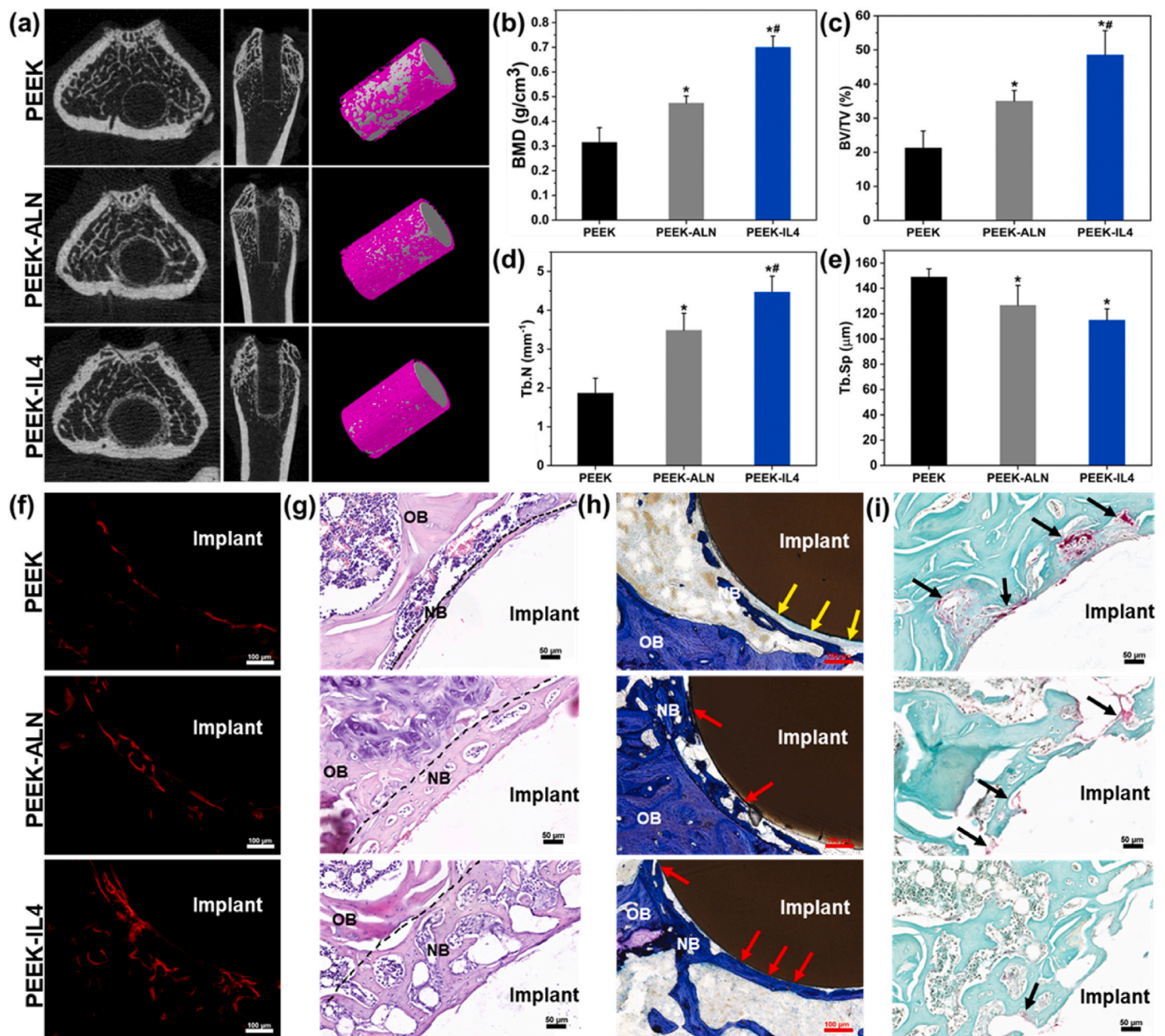
Fig. 7. *In vivo* bone regeneration under osteoporotic conditions after implantation for 4 weeks: (a) Reconstructed transverse, coronal, and 3D micro-CT images; (b–e) Quantitative analysis of the micro-CT data including (b) BMD, (c) BV/TV, (d) Tb.N and (e) Tb.Sp (n = 5 per group); (f) Red fluorescent labeling of new bone formation surrounding the implants; (g) Histological observation of the peri-implant tissues after H&E staining with new bones marked by dashed lines; (h) Histological observation of the peri-implant tissues after toluidine blue staining; (i) Histological observation of the peri-implant tissues after TRAP staining. OB, old bone; NB, new bone; Yellow arrows mark the fibrous capsule; Red arrows mark the direct contact between new bone and the implants; Black arrows mark the TRAP positive cells. $*p < 0.05$ compared to PEEK, $\#p < 0.05$ compared to PEEK-ALN.

process is tracked by fluorescent labeling using alizarin red. As shown in Fig. 7f and Fig. S14, the percentage of stained bone area follows the same trend of PEEK-IL4 > PEEK-ALN > PEEK. Fig. 7g and h show the results of H&E staining and toluidine blue staining, respectively. Consistent with micro-CT scanning and fluorescent labeling, H&E staining and toluidine blue staining reveal that the layer of new bone around the PEEK-IL4 implant is much thicker than that in the other groups. In addition, the percentage of bone-implant contact follows the trend of PEEK-IL4 > PEEK-ALN > PEEK (Fig. S15). Notably, most of the newly formed bone bonds directly with the PEEK-IL4 implant (marked by red arrows), whereas fibrous connective tissues (marked by yellow arrows) are observed from the bone-implant interface after implantation of PEEK.

With regard to osteoclastogenesis *in vivo*, the sections obtained from different groups are studied by TRAP staining. As shown in Fig. 7h, the periphery of PEEK-IL4 implant shows the smallest number of TRAP-positive cells (marked by black arrows) among the 3 groups, indicating that the PEEK-IL4 implant with a programmed surface can enhance the bone regeneration process by improving osteogenesis and attenuating osteoclastogenesis at the same time.

The results reveal our innovative attempt of programming the surface of PEEK to ameliorate bone-implant osseointegration under osteoporotic conditions by initiating immunomodulation and fostering bone regeneration thereafter. The cascade of IL-4 and a small amount of ALN and Ca^{2+} in the early stage after implantation creates an osteoimmunomodulatory microenvironment. In the following weeks, steady release

of ALN and Ca^{2+} boosts osteogenesis and suppresses osteoclastogenesis continuously, contributing to new bone formation at the bone-implant interface with high quantity and quality. As a consequence, success of bone implantation can be achieved even under osteoporotic conditions.

4. Conclusion

A programmed surface is designed and constructed on PEEK to dictate immune-mediated peri-implant bone regeneration. In the early stage after implantation, dominant release of IL-4 and a handful of ALN and Ca^{2+} mitigate the acute inflammatory reaction by promoting M2 polarization of macrophages, creating a desirable osteoimmunomodulatory microenvironment. In the following weeks, slow and sustained release of ALN and Ca^{2+} restores the balance between osteogenesis and osteoclastogenesis to foster peri-implant bone formation even under osteoporotic conditions. As a result, bones with high quantity and quality are formed onto the implant with programmed surface and solid bone-implant osseointegration is accomplished. This novel strategy of sequential functionalization has great potential in clinical applications and also provides insights into the design of advanced orthopedic implants especially for osteoporotic patients.

Data availability

The data are available from the corresponding author on reasonable request.

CRediT authorship contribution statement

Yanyan Zheng: Investigation, Writing – original draft. **Ang Gao:** Methodology, Writing – review & editing. **Jiaxiang Bai:** Validation, Formal analysis. **Qing Liao:** Methodology, Investigation. **Yuzheng Wu:** Formal analysis. **Wei Zhang:** Writing – review & editing. **Min Guan:** Visualization, Project administration. **Liping Tong:** Conceptualization, Supervision. **Dechun Geng:** Conceptualization, Supervision. **Xin Zhao:** Visualization, Writing – review & editing. **Paul K. Chu:** Conceptualization, Writing – review & editing. **Huaiyu Wang:** Conceptualization, Supervision, Funding acquisition.

Declaration of competing interest

The authors declare no conflict of interest.

Acknowledgements

Appendix A. Supplementary data

Supplementary data to this article can be found online at https://doi.org/10.1016/j.bioactmat.2022.01.042.

References

[1] M. He, Y. Huang, H. Xu, G. Feng, L. Liu, Y. Li, D. Sun, L. Zhang, Modification of polyetheretherketone implants: from enhancing bone integration to enabling multi-modal therapeutics, Acta Biomater. 129 (2021) 18–32.

[2] F.B. Torstrick, A.S.P. Lin, D. Potter, D.L. Safranski, T.A. Sulchek, K. Gall, R. E. Guldberg, Porous PEEK improves the bone-implant interface compared to plasma-sprayed titanium coating on PEEK, Biomaterials 185 (2018) 106–116.

[3] S.M. Kurtz, J.N. Devine, PEEK biomaterials in trauma, orthopedic, and spinal implants, Biomaterials 28 (32) (2007) 4845–4869.

[4] X. Wang, J. Guo, J. Wen, X. Zhang, L. Cao, D. Zeng, X. Liu, X. Jiang, Novel vascular strategies on polyetheretherketone modification in promoting osseointegration in ovariectomized rats, Mater. Des. 202 (2021) 109526.

[5] Y. Zheng, C. Xiong, Z. Wang, X. Li, L. Zhang, A combination of CO_2 laser and plasma surface modification of poly(etheretherketone) to enhance osteoblast response, Appl. Surf. Sci. 344 (2015) 79–88, 0.

[6] S. Mo, F. Zhao, A. Gao, Y. Wu, Q. Liao, L. Xie, H. Pan, L. Tong, P.K. Chu, H. Wang, Simultaneous application of diamond-like carbon coating and surface amination on polyether ether ketone: towards superior mechanical performance and osseointegration, Smart. Mater.Med. 2 (2021) 219–228.

[7] T. Lu, J. Wen, S. Qian, H. Cao, C. Ning, X. Pan, X. Jiang, X. Liu, P.K. Chu, Enhanced osteointegration on tantalum-implanted polyetheretherketone surface with bone-like elastic modulus, Biomaterials 51 (2015) 173–183, 0.

[8] H. Mahjoubi, E. Buck, P. Manimunda, R. Farivar, R. Chromik, M. Murshed, M. Cerruti, Surface phosphonation enhances hydroxyapatite coating adhesion on polyetheretherketone and its osseointegration potential, Acta Biomater. 47 (2017) 149–158.

[9] X. Yuan, L. Ouyang, Y. Luo, Z. Sun, C. Yang, J. Wang, X. Liu, X. Zhang, Multifunctional sulfonated polyetheretherketone coating with beta-defensin-14 for yielding durable and broad-spectrum antibacterial activity and osseointegration, Acta Biomater. 86 (2019) 323–337.

[10] Y. Zheng, L. Liu, L. Xiao, Q. Zhang, Y. Liu, Enhanced osteogenic activity of phosphorylated polyetheretherketone via surface-initiated grafting polymerization of vinylphosphonic acid, Colloids Surf. B Biointerfaces 173 (2019) 591–598.

[11] B.N. Brown, B.D. Ratner, S.B. Goodman, S. Amar, S.F. Badylak, Macrophage polarization: an opportunity for improved outcomes in biomaterials and regenerative medicine, Biomaterials 33 (15) (2012) 3792–3802.

[12] Z. Chen, J. Yuen, R. Crawford, J. Chang, C. Wu, Y. Xiao, The effect of osteoimmunomodulation on the osteogenic effects of cobalt incorporated β-tricalcium phosphate, Biomaterials 61 (2015) 126–138.

[13] N. Kohli, S. Ho, S.J. Brown, P. Sawadkar, V. Sharma, M. Snow, E. García-Gareta, Bone remodelling in vitro: where are we headed ? -A review on the current understanding of physiological bone remodelling and inflammation and the strategies for testing biomaterials in vitro, Bone 110 (2018) 38–46.

[14] Z. Chen, T. Klein, R.Z. Murray, R. Crawford, J. Chang, C. Wu, Y. Xiao, Osteoimmunomodulation for the development of advanced bone biomaterials, Mater. Today 19 (6) (2016) 304–321.

[15] L. Bai, Z. Du, J. Du, W. Yao, J. Zhang, Z. Weng, S. Liu, Y. Zhao, Y. Liu, X. Zhang, X. Huang, X. Yao, R. Crawford, R. Hang, D. Huang, B. Tang, Y. Xiao, A multifaceted coating on titanium dictates osteoimmunomodulation and osteo/angio-genesis towards ameliorative osseointegration, Biomaterials 162 (2018) 154–169.

[16] L. Xie, G. Wang, Y. Wu, Q. Liao, S. Mo, X. Ren, L. Tong, W. Zhang, M. Guan, H. Pan, P.K. Chu, H. Wang, Programmed surface on poly(aryl-ether-ether-ketone) initiating immune mediation and fulfilling bone regeneration sequentially, Innovation 2 (3) (2021) 100148.

[17] A. Gao, Q. Liao, L. Xie, G. Wang, W. Zhang, Y. Wu, P. Li, M. Guan, H. Pan, L. Tong, P.K. Chu, H. Wang, Tuning the surface immunomodulatory functions of polyetheretherketone for enhanced osseointegration, Biomaterials 230 (2020) 119642.

[18] Q.-L. Ma, L.-Z. Zhao, R.-R. Liu, B.-Q. Jin, W. Song, Y. Wang, Y.-S. Zhang, L.-H. Chen, Y.-M. Zhang, Improved implant osseointegration of a nanostructured titanium surface via mediation of macrophage polarization, Biomaterials 35 (37) (2014) 9853–9867.

[19] R. Siqueira, J.A. Ferreira, F.A.P. Rizzante, G.F. Moura, D.B.S. Mendonça, D. de Magalhães, R. Cimões, G. Mendonça, Hydrophilic titanium surface modulates early stages of osseointegration in osteoporosis, J. Periodontal. Res. 56 (2) (2021) 351–362.

[20] H. Bai, Y. Cui, C. Wang, Z. Wang, W. Luo, Y. Liu, Y. Leng, J. Wang, Z. Li, H. Liu, 3D printed porous biomimetic composition sustained release zoledronate to promote osteointegration of osteoporotic defects, Mater. Des. 189 (2020) 108513.

[21] E.M. Lotz, D.J. Cohen, R.A. Ellis, J.S. Wayne, Z. Schwartz, B.D. Boyan, Ibandronate Treatment before and after implant insertion impairs osseointegration in aged rats with ovariectomy induced osteoporosis, JBMR Plus 3 (7) (2019), e10184.

[22] P. Gentile, V. Chiono, I. Carmagnola, P.V. Hatton, An overview of poly(lactic-co-glycolic) acid (PLGA)-based biomaterials for bone tissue engineering, Int. J. Mol. Sci. 15 (3) (2014) 3640–3659.

[23] H.K. Makadia, S.J. Siegel, Poly Lactic-co-Glycolic Acid (PLGA) as biodegradable controlled drug delivery carrier, Polymers 3 (3) (2011) 1377–1397.

[24] M.J. Rogers, J. Mönkkönen, M.A. Munoz, Molecular mechanisms of action of bisphosphonates and new insights into their effects outside the skeleton, Bone 139 (2020) 115493.

[25] M. Li, P. Xiong, F. Yan, S. Li, C. Ren, Z. Yin, A. Li, H. Li, X. Ji, Y. Zheng, Y. Cheng, An overview of graphene-based hydroxyapatite composites for orthopedic applications, Bioact. Mater. 3 (1) (2018) 1–18.

[26] Z.-W. Zheng, Y.-H. Chen, D.-Y. Wu, J.-B. Wang, M.-M. Lv, X.-S. Wang, J. Sun, Z.-Y. Zhang, Development of an accurate and proactive immunomodulatory strategy

to improve bone substitute material-mediated osteogenesis and angiogenesis, Theranostics 8 (19) (2018) 5482–5500.

[27] M. Li, F. Wei, X. Yin, L. Xiao, L. Yang, J. Su, J. Weng, B. Feng, Y. Xiao, Y. Zhou, Synergistic regulation of osteoimmune microenvironment by IL-4 and RGD to accelerate osteogenesis, Mater. Sci. Eng. C. Mater. Biol. Appl. 109 (2020) 110508.

[28] J. Kuljanin, I. Janković, J. Nedeljković, D. Prstojević, V. Marinković, Spectrophotometric determination of alendronate in pharmaceutical formulations via complex formation with Fe(III) ions, J. Pharmaceut. Biomed. Anal. 28 (6) (2002) 1215–1220.

[29] A. Gao, R. Hang, W. Li, W. Zhang, P. Li, G. Wang, L. Bai, X.-F. Yu, H. Wang, L. Tong, P.K. Chu, Linker-free covalent immobilization of heparin, SDF-1α, and CD47 on PTFE surface for antithrombogenicity, endothelialization and anti-inflammation, Biomaterials 140 (2017) 201–211.

[30] S.C. Funes, M. Rios, J. Escobar-Vera, A.M. Kalergis, Implications of macrophage polarization in autoimmunity, Immunology 154 (2) (2018) 186–195.

[31] J. Lee, H. Byun, S.K. Madhurakkat Perikamana, S. Lee, H. Shin, Current advances in immunomodulatory biomaterials for bone regeneration, Adv. Healthc. Mater. 8 (4) (2019) 1801106.

[32] D. Hachim, S.T. LoPresti, C.C. Yates, B.N. Brown, Shifts in macrophage phenotype at the biomaterial interface via IL-4 eluting coatings are associated with improved implant integration, Biomaterials 112 (2017) 95–107.

[33] K.L. Spiller, S. Nassiri, C.E. Witherel, R.R. Anfang, J. Ng, K.R. Nakazawa, T. Yu, G. Vunjak-Novakovic, Sequential delivery of immunomodulatory cytokines to facilitate the M1-to-M2 transition of macrophages and enhance vascularization of bone scaffolds, Biomaterials 37 (2015) 194–207.

[34] S. Hamlet, S. Ivanovski, Inflammatory cytokine response to titanium chemical composition and nanoscale calcium phosphate surface modification, Acta Biomater. 7 (5) (2011) 2345–2353.

[35] Y. Liu, F. Shi, K. Gong, Y. Liu, W. Zhi, J. Weng, S. Qu, Study on critical-sized ultra-high molecular weight polyethylene wear particles loaded with alendronate sodium: in vitro release and cell response, J. Mater. Sci. Mater. Med. 28 (4) (2017) 56.

[36] L. Xiao, Y. Xiao, The autophagy in osteoimmonology: self-eating, maintenance, and beyond, Front. Endocrinol. 10 (2019) 490.

[37] M.B. Asparuhova, J. Caballé-Serrano, D. Buser, V. Chappuis, Bone-conditioned medium contributes to initiation and progression of osteogenesis by exhibiting synergistic TGF-β1/BMP-2 activity, Int. J. Oral Sci. 10 (2) (2018) 20.

[38] R. Derynck, Y.E. Zhang, Smad-dependent and Smad-independent pathways in TGF-β family signalling, Nature 425 (6958) (2003) 577–584.

[39] L.N. Ramoshebi, T.N. Matsaba, J. Teare, L. Renton, J. Patton, U. Ripamonti, Tissue engineering: TGF-β superfamily members and delivery systems in bone regeneration, Expet Rev. Mol. Med. 4 (20) (2002) 1–11.

[40] Q. Ma, N. Jiang, S. Liang, F. Chen, L. Fang, X. Wang, J. Wang, L. Chen, Functionalization of a clustered TiO$_2$ nanotubular surface with platelet derived growth factor-BB covalent modification enhances osteogenic differentiation of bone marrow mesenchymal stem cells, Biomaterials 230 (2020) 119650.

[41] S.-y. Gao, R.-b. Lin, S.-h. Huang, Y.-j. Liang, X. Li, S.-e. Zhang, D.-q. Ouyang, K. Li, G.-s. Zheng, G.-q. Liao, PDGF-BB exhibited therapeutic effects on rat model of bisphosphonate-related osteonecrosis of the jaw by enhancing angiogenesis and osteogenesis, Bone 144 (2021) 115117.

[42] A.I. Caplan, D. Correa, PDGF in bone formation and regeneration: new insights into a novel mechanism involving MSCs, J. Orthop. Res. 29 (12) (2011) 1795–1803.

[43] L. Bacakova, E. Filova, M. Parizek, T. Ruml, V. Svorcik, Modulation of cell adhesion, proliferation and differentiation on materials designed for body implants, Biotechnol. Adv. 29 (6) (2011) 739–767.

[44] X. Shen, P. Ma, Y. Hu, G. Xu, K. Xu, W. Chen, Q. Ran, L. Dai, Y. Yu, C. Mu, K. Cai, Alendronate-loaded hydroxyapatite-TiO$_2$ nanotubes for improved bone formation in osteoporotic rabbits, J. Mater. Chem. B 4 (8) (2016) 1423–1436.

[45] L. Fan, P. Guan, C. Xiao, H. Wen, Q. Wang, C. Liu, Y. Luo, L. Ma, G. Tan, P. Yu, L. Zhou, C. Ning, Exosome-functionalized polyetheretherketone-based implant with immunomodulatory property for enhancing osseointegration, Bioact. Mater. 6 (9) (2021) 2754–2766.

[46] Y. Liu, F. Shi, L. Bo, W. Zhi, J. Weng, S. Qu, A novel alginate-encapsulated system to study biological response to critical-sized wear particles of UHMWPE loaded with alendronate sodium, Mater. Sci. Eng. C 79 (2017) 679–686.

[47] W. Zhang, F. Zhao, D. Huang, X. Fu, X. Li, X. Chen, Strontium-substituted submicrometer bioactive glasses modulate macrophage responses for improved bone regeneration, ACS Appl. Mater. Interfaces 8 (45) (2016) 30747–30758.

[48] Y. Zeng, M. Zhou, L. Chen, H. Fang, S. Liu, C. Zhou, J. Sun, Z. Wang, Alendronate loaded graphene oxide functionalized collagen sponge for the dual effects of osteogenesis and anti-osteoclastogenesis in osteoporotic rats, Bioact. Mater. 5 (4) (2020) 859–870.

[49] X. Chen, Z. Wang, N. Duan, G. Zhu, E.M. Schwarz, C. Xie, Osteoblast–osteoclast interactions, Connect. Tissue Res. 59 (2) (2018) 99–107.

[50] M. Lind, B. Deleuran, H. Yssel, E. Fink-Eriksen, K. Thestrup-Pedersen, IL-4 and IL-13, but not IL-10, are chemotactic factors for human osteoblasts, Cytokine 7 (1) (1995) 78–82.

[51] K. Nohtomi, K. Sato, K. Shizume, K. Yamazaki, H. Demura, K. Hosoda, Y. Murata, H. Seo, Stimulation of interleukin-4 of cell proliferation and mRNA expression of alkaline phosphatase and collagen type I in human osteoblast-like cells of trabecular bone, Bone Miner. 27 (1) (1994) 69–79.

[52] C.-J. Silfverswärd, H. Penno, A. Frost, O. Nilsson, Ö. Ljunggren, Expression of markers of activity in cultured human osteoblasts: effects of interleukin-4 and interleukin-13, Scand. J. Clin. Lab. Investig. 70 (5) (2010) 338–342.

[53] J. Cheng, J. Liu, Z. Shi, D. Xu, S. Luo, G.P. Siegal, X. Feng, S. Wei, Interleukin-4 inhibits RANKL-induced NFATc1 expression via STAT6: a novel mechanism mediating its blockade of osteoclastogenesis, J. Cell. Biochem. 112 (11) (2011) 3385–3392.

[54] Y. Hu, B. Ek-Rylander, M. Wendel, G. Andersson, Reciprocal effects of Interferon-γ and IL-4 on differentiation to osteoclast-like cells by RANKL or LPS, Oral Dis. 20 (7) (2014) 682–692.

[55] H.S. Alghamdi, R. Bosco, S.K. Both, M. Iafisco, S.C.G. Leeuwenburgh, J.A. Jansen, J.J.J.P. van den Beucken, Synergistic effects of bisphosphonate and calcium phosphate nanoparticles on peri-implant bone responses in osteoporotic rats, Biomaterials 35 (21) (2014) 5482–5490.

[56] S. Tarafder, S. Bose, Polycaprolactone-coated 3D printed tricalcium phosphate scaffolds for bone tissue engineering: in vitro alendronate release behavior and local delivery effect on *in vivo* osteogenesis, ACS Appl. Mater. Interfaces 6 (13) (2014) 9955–9965.

[57] B. Cai, P. Tan, N. Jiang, Z. Guo, B. Ay, S. Li, Y. Hou, Y. Li, Y. You, L. Zhang, S. Zhu, Bioinspired fabrication of calcium-doped TiP coating with nanofibrous microstructure to accelerate osseointegration, Bioconjugate Chem. 31 (6) (2020) 1641–1650.

[58] A. Montaseri, C. Giampietri, M. Rossi, A. Riccioli, A. Del Fattore, A. Filippini, The role of autophagy in osteoclast differentiation and bone resorption function, Biomolecules 10 (10) (2020) 1398.

[59] R.-F. Li, G. Chen, J.-G. Ren, W. Zhang, Z.-X. Wu, B. Liu, Y. Zhao, Y.-F. Zhao, The adaptor protein p62 is involved in RANKL-induced autophagy and osteoclastogenesis, J. Histochem. Cytochem. 62 (12) (2014) 879–888.

[60] X. Xu, Y. Li, L. Wang, Y. Li, J. Pan, X. Fu, Z. Luo, Y. Sui, S. Zhang, L. Wang, Y. Ni, L. Zhang, S. Wei, Triple-functional polyetheretherketone surface with enhanced bacteriostasis and anti-inflammatory and osseointegrative properties for implant application, Biomaterials 212 (2019) 98–114.

[61] D. Zhang, Q. Chen, C. Shi, M. Chen, K. Ma, J. Wan, R. Liu, Dealing with the foreign-body response to implanted biomaterials: strategies and applications of new materials, Adv. Funct. Mater. 31 (2020) 2007226.